Stochastic Optimal Control Model for Natural Gas Network Operations[*]

Victor M. Zavala

Mathematics and Computer Science Division

Argonne National Laboratory, 9700 South Cass Avenue, Argonne, IL 60439, USA

Abstract

We present a stochastic optimal control model to optimize gas network inventories in the face of system uncertainties. The model captures detailed network dynamics and operational constraints and uses a weighted risk-mean objective. We perform a degrees-of-freedom analysis to assess operational flexibility and to determine conditions for model consistency. We compare the control policies obtained with the stochastic model against those of deterministic and robust counterparts. In addition, we demonstrate that the use of risk metrics can help operators to systematically mitigate system volatility. Moreover, we discuss computational scalability issues and effects of discretization resolution on economic performance.

1 Introduction

Consider a gas network with links comprising of long pipelines and nodes consisting of junction points and compressors. Gas is withdrawn from the network at a set of demand nodes and make-up gas is brought into the system through a set of supply nodes. In a real-time environment, the system operator must balance the network to satisfy demand flows and delivery pressures at all times. To achieve this balance, compressors are operated to coordinate buildup and release of inventory inside the pipes. This procedure, called "line-pack management" [20], consists on determining dynamic operating policies for the compressors to balance supply, inventory, and demand. The policies must respect compression limits and minimize compressor power or fuel. One of the key issues arising in operations is that demand profiles cannot be predicted with full certainty and thus inventory must be built up, *in advance*, to ensure that enough capacity is available to satisfy a range of possible future scenarios. Uncertainty in gas pipeline operations is becoming an increasing concern as the power grid adopts larger amounts of intermittent weather-driven resources, because gas-fired power plant units are typically used to balance supply at short notice [13, 20].

Optimization of gas networks has been performed in diverse studies. These studies differ in the decision setting and physical models used. Optimization models for mid-term planning and contracting purposes do not require information about line-pack dynamics so steady-state models are appropriate. O'Neill et.al. [18] present a steady-state optimization model for transmission of natural gas. Wolf and Smeers [7] present a nonlinear steady-state transmission model and develop an extension of the simplex method to solve it. An optimal design model for pipes diameters is proposed by the same authors in [6]. Martin et.al. [15] present a steady-state nonlinear transmission model that allows for hybrid (on/off) decisions (a mixed-integer

nonlinear optimization model) and develop strategies to approximate nonlinear terms using piecewise linear functions, thus enabling the use of mixed-integer linear programming solvers.

For real-time operations system dynamics must be captured in order to ensure feasible and implementable policies. Moritz [16] presents a mixed-integer optimal control model with detailed conservation and momentum equations, network balances, and hybrid valve and compressor components. As the author acknowledges, however, computational limitations forced her to consider conservation and momentum equations in simplified form, by defining only inlet and output points. This is equivalent to discretizing the underlying partial differential equations (PDEs) using two discretization points placed at the boundary nodes. Ehrhardt and Steinbach [9] present a nonlinear continuous optimal control model in which compressor policies are optimized to satisfy demands and minimize compressor fuel. A full space-time discretization of the PDEs is performed and a sequential quadratic programming algorithm is used for the solution of the resulting nonlinear programming (NLP) problem. Steinbach and Ehrhardt [23] proposed the use of an interior point algorithm to solve the NLP and they propose a strategy to exploit the space-time linear algebra structure. These studies focused on computational performance, with limited modeling and economic performance analysis. Baumrucker and Biegler [1] present an optimal control formulation allowing for hybrid behavior arising from flow reversals. The authors propose a mathematical program with equilibrium constraints formulation and analyze the effect of different electricity price structures on economic performance.

None of the real-time optimization models presented in the literature account for uncertainty, with the exception of the work of Carter and Rachford [3]. In their work, they present a detailed discussion of uncertainties prevailing in real-time operations and discuss the benefits of using stochastic optimization formulations to manage line-pack inventory. The authors provide a sound physical analysis of the resulting optimal policies; however, they do not report the model and solution strategy used.

In this work, we present a detailed stochastic optimal control model that considers conservation and momentum equations, typical operational constraints, and uncertainty in demands. We perform a degrees-of-freedom (DOF) analysis to verify the consistency of the model and we use this analysis to derive consistent initial conditions and nonanticipacity constraints. In addition, we propose to incorporate a risk metric into the objective function to mitigate cost variance and system volatility. Using a computational study, we demonstrate the benefits obtained with stochastic formulations against deterministic and robust counterparts and we discuss the effects of discretization mesh resolution on economic performance.

The paper is structured as follows. In Section 2 we present the physical model for the pipelines, network, and compressors. In Section 3 we present a degrees-of-freedom (DOF) analysis to characterize the differential and algebraic equation (DAE) system and provide conditions to achieve model consistency. In Section 4 we formulate the stochastic optimal control model by defining the objective function, operational constraints, initial conditions, and nonanticipativity constraints. In Section 5 we present a computational study to demonstrate the benefits of the stochastic model over a range of different formulations and we discuss computational issues. The paper closes in Section 6 with concluding remarks and directions of future work. The model nomenclature as well as variables and parameter units are presented in Appendix A.

2 Physical Model

In this section, we present the conservation and momentum equations governing the dynamics of each pipeline in the network, and we provide equations describing the network interconnections. Nomenclature, physical units, and typical values for all variables and parameters are given in Appendix A.

2.1 Conservation, Momentum, and Network

We assume an isothermal and ideal gas flow through a horizontal pipe and define a set $\mathcal{L}$ of pipes or links. The conservation and momentum equations for a given link $\ell \in \mathcal{L}$ are given by the following set of PDEs [24, 19]:

$$\frac{\partial \rho_\ell(\tau, x, \omega)}{\partial \tau} + \frac{\partial(\rho_\ell(\tau, x, \omega) w_\ell(\tau, x, \omega))}{\partial x} = 0 \tag{2.1a}$$

$$\frac{\partial(\rho_\ell(\tau, x, \omega) w_\ell(\tau, x, \omega))}{\partial \tau} + \frac{\partial p_\ell(\tau, x, \omega)}{\partial x} = -\frac{\lambda_\ell}{2 D_\ell} \rho_\ell(\tau, x, \omega) w_\ell(\tau, x, \omega) |w_\ell(\tau, x, \omega)|. \tag{2.1b}$$

Here, $\tau \in \mathcal{T} := [0, T]$ is the time dimension with final time T (planning horizon), and $x \in \mathcal{X}_\ell := [0, L_\ell]$ is the axial dimension with length L_ℓ. We also define a set of scenarios $\omega \in \Omega := \{1..N_\Omega\}$. The link diameters are denoted as D_ℓ and the friction coefficients are denoted as λ_ℓ. The states of the link are the gas density $\rho_\ell(\tau, x, \omega)$, the gas speed $w_\ell(\tau, x, \omega)$, and the gas pressure $p_\ell(\tau, x, \omega)$. The transversal area A_ℓ, volumetric flow $q_\ell(\tau, x, \omega)$, and mass flow $f_\ell(\tau, x, \omega)$ are given by

$$A_\ell = \frac{1}{4} \pi D_\ell^2 \tag{2.2a}$$

$$q_\ell(\tau, x, \omega) = w_\ell(\tau, x, \omega) \, A_\ell \tag{2.2b}$$

$$f_\ell(\tau, x, \omega) = \rho_\ell(\tau, x, \omega) \, w_\ell(\tau, x, \omega) \, A_\ell. \tag{2.2c}$$

Pressure and density are related as follows:

$$\frac{p_\ell(\tau, x, \omega)}{\rho_\ell(\tau, x, \omega)} = \nu^2. \tag{2.3}$$

Here, ν is the speed of sound in the gas. We transform (2.1) into a more convenient form in terms of mass flow and pressure by using (2.3) and (2.2):

$$\frac{\partial p_\ell(\tau, x, \omega)}{\partial \tau} + \frac{\nu^2}{A_\ell} \frac{\partial f_\ell(\tau, x, \omega)}{\partial x} = 0 \tag{2.4a}$$

$$\frac{1}{A_\ell} \frac{\partial f_\ell(\tau, x, \omega)}{\partial \tau} + \frac{\partial p_\ell(\tau, x, \omega)}{\partial x} = -\frac{\lambda_\ell \rho_\ell(\tau, x, \omega)}{2 D_\ell} \frac{f_\ell(\tau, x, \omega)}{\rho_\ell(\tau, x, \omega) \, A_\ell} \left| \frac{f_\ell(\tau, x, \omega)}{\rho_\ell(\tau, x, \omega) \, A_\ell} \right|. \tag{2.4b}$$

Substituting (2.3) and (2.2a) in (2.4b) and performing some manipulations, we obtain the more compact form,

$$\frac{\partial p_\ell(\tau, x, \omega)}{\partial \tau} = -\frac{\nu^2}{A_\ell} \frac{\partial f_\ell(\tau, x, \omega)}{\partial x} \tag{2.5a}$$

$$\frac{1}{A_\ell} \frac{\partial f_\ell(\tau, x, \omega)}{\partial \tau} = -\frac{\partial p_\ell(\tau, x, \omega)}{\partial x} - \frac{8 \, \lambda_\ell \, \nu^2}{\pi^2 \, D_\ell^5} \frac{f_\ell(\tau, x, \omega) |f_\ell(\tau, x, \omega)|}{p_\ell(\tau, x, \omega)}. \tag{2.5b}$$

For numerical purposes, we define scaled flows $f_\ell(\tau, x, \omega) \leftarrow \alpha_f f_\ell(\tau, x, \omega)$ and pressures $p_\ell(\tau, x, \omega) \leftarrow \alpha_p p_\ell(\tau, x, \omega)$, where α_f and α_p are scaling factors. Scaling (2.5) and rearranging, we obtain

$$\frac{\partial p_\ell(\tau, x, \omega)}{\partial \tau} = -c_{1,\ell} \frac{\partial f_\ell(\tau, x, \omega)}{\partial x}, \quad \ell \in \mathcal{L}, \tau \in \mathcal{T}, x \in \mathcal{X}_\ell, \omega \in \Omega \tag{2.6a}$$

$$\frac{\partial f_\ell(\tau, x, \omega)}{\partial \tau} = -c_{2,\ell} \frac{\partial p_\ell(\tau, x, \omega)}{\partial x} - c_{3,\ell} \frac{f_\ell(\tau, x, \omega) |f_\ell(\tau, x, \omega)|}{p_\ell(\tau, x, \omega)}, \quad \ell \in \mathcal{L}, \tau \in \mathcal{T}, x \in \mathcal{X}_\ell, \omega \in \Omega, \tag{2.6b}$$

3

where the constants $c_{1,\ell}, c_{2,\ell}$, and $c_{3,\ell}$ are defined in Appendix A.

We now consider a network with a set $\mathcal{N}$ of nodes, a set $\mathcal{L}$ of links, a set $\mathcal{S}$ of supply flows, and a set $\mathcal{D}$ of demand flows. For each node $n \in \mathcal{N}$ we define the set of inlet and outlet links, $\mathcal{L}_n^{in} := \{\ell \mid rec(\ell) = n\}, \mathcal{L}_n^{out} := \{\ell \mid snd(\ell) = n\}$. Here, $rec(\ell)$ is the receiving node of link ℓ and $snd(\ell)$ is the sending node of link ℓ. We define $dem(j)$ as the node at which the demand flow $d_j(\tau, \omega)$ is located and $sup(i)$ as the node at which the supply flow $s_i(\tau, \omega)$ is located. Accordingly, we define the sets For $\mathcal{S}_n := \{j \in \mathcal{S} \mid sup(j) = n\}$ and $\mathcal{D}_n := \{j \in \mathcal{D} \mid dem(j) = n\}$ for each node $n \in \mathcal{N}$.

For modeling convenience, we avoid direct linking of the link flows at the nodes. Instead, we introduce *dummy* inlet and outlet flow states for each link $f_\ell^{in}(\tau, \omega)$ and $f_\ell^{out}(\tau, \omega)$, respectively. In Section 3 we will see that this modification does not affect the consistency of the model. The flow balances at the nodes are given by,

$$\sum_{\ell \in \mathcal{L}_n^{in}} f_\ell^{in}(\tau, \omega) - \sum_{\ell \in \mathcal{L}_n^{out}} f_\ell^{out}(\tau, \omega) + \sum_{i \in \mathcal{S}_n} s_i(\tau, \omega) - \sum_{j \in \mathcal{D}_n} d_j(\tau, \omega) = 0, \ n \in \mathcal{N}, \tau \in \mathcal{T}, \omega \in \Omega. \tag{2.7}$$

The boundary conditions for the link flows can now be specified by using the dummy flows,

$$f_\ell(\tau, L_\ell, \omega) = f_\ell^{out}(\tau, \omega), \ \ell \in \mathcal{L}, \tau \in \mathcal{T}, \omega \in \Omega \tag{2.8a}$$

$$f_\ell(\tau, 0, \omega) = f_\ell^{in}(\tau, \omega), \ \ell \in \mathcal{L}, \tau \in \mathcal{T}, \omega \in \Omega. \tag{2.8b}$$

We assume that the direction of the flows is given. Computational strategies to allow for flow reversals are proposed in [1].

2.2 Compressors

To link pressures, we define the pressures at the nodes as $\theta_n(\tau), n \in \mathcal{N}$, and we split the set of links $\mathcal{L}$ into subsets of passive $\mathcal{L}_p$ links and active links $\mathcal{L}_a$. For the active links, we define the boost pressures $\Delta\theta_\ell(\tau)$, which is the additional (non-negative) pressure introduced by the compressor located at the inlet (sending) node of the link. For the passive links, there is no compression. The boundary conditions for the link pressures are given by

$$p_\ell(\tau, L_\ell, \omega) = \theta_{rec(\ell)}(\tau, \omega), \ \ell \in \mathcal{L}, \tau \in \mathcal{T}, \omega \in \Omega \tag{2.9a}$$

$$p_\ell(\tau, 0, \omega) = \theta_{snd(\ell)}(\tau, \omega), \ \ell \in \mathcal{L}_p, \tau \in \mathcal{T}, \omega \in \Omega \tag{2.9b}$$

$$p_\ell(\tau, 0, \omega) = \theta_{snd(\ell)}(\tau, \omega) + \Delta\theta_\ell(\tau), \ \ell \in \mathcal{L}_a, \tau \in \mathcal{T}, \omega \in \Omega. \tag{2.9c}$$

The total power consumed in the active links, $P_\ell(\tau, \omega)$, is computed from

$$P_\ell(\tau, \omega) = c_4 \, f_\ell^{in}(\tau, \omega) \left(\left(\frac{\theta_{snd(\ell)}(\tau, \omega) + \Delta\theta_\ell(\tau, \omega)}{\theta_{snd(\ell)}(\tau, \omega)} \right)^\beta - 1 \right), \ \ell \in \mathcal{L}_a, \tau \in \mathcal{T}, \omega \in \Omega, \tag{2.10}$$

where c_4 is a constant defined in Appendix A.

3 DOF Analysis

In this section, we perform a DOF analysis to determine conditions for consistency of the physical model and to determine appropriate initial conditions. For clarity in the presentation, we consider a discretized version of the conservation, momentum, and network equations. Assume that the PDEs of each link are

discretized in space by using a finite difference scheme using N_x points of equal length Δx_ℓ and discretized in time by using an implicit Euler scheme with N_t points of equal length $\Delta \tau$ [23]. We define the sets $\bar{\mathcal{X}} := \{1, ..., N_x\}$, $\bar{\mathcal{T}} := \{1, ..., N_t\}$, $\bar{\mathcal{X}}^- := \{1, ..., N_x - 1\}$, and $\bar{\mathcal{T}}^- := \{1, ..., N_t - 1\}$. The discretized version of the physical model given by equations (2.6)-(2.10) is,

$$0 = \sum_{\ell \in \mathcal{L}_n^{in}} f_{\ell,t}^{in}(\omega) - \sum_{\ell \in \mathcal{L}_n^{out}} f_{\ell,t}^{out}(\omega) + \sum_{i \in \mathcal{S}_n} s_{i,t}(\omega) - \sum_{j \in \mathcal{D}_n} d_{j,t}(\omega), \ n \in \mathcal{N}, t \in \bar{\mathcal{T}}, \omega \in \Omega \tag{3.11a}$$

$$\frac{p_{\ell,t+1,k}(\omega) - p_{\ell,t,k}(\omega)}{\Delta \tau} = -c_{1,\ell} \frac{f_{\ell,t+1,k+1}(\omega) - f_{\ell,t+1,k}(\omega)}{\Delta x_\ell}, \ \ell \in \mathcal{L}, t \in \bar{\mathcal{T}}^-, k \in \bar{\mathcal{X}}^-, \omega \in \Omega \tag{3.11b}$$

$$\frac{f_{\ell,t+1,k}(\omega) - f_{\ell,t,k}(\omega)}{\Delta \tau} = -c_{2,\ell} \frac{p_{\ell,t+1,k+1}(\omega) - p_{\ell,t+1,k}(\omega)}{\Delta x_\ell}$$
$$- c_{3,\ell} \frac{f_{\ell,t+1,k}(\omega)|f_{\ell,t+1,k}(\omega)|}{p_{\ell,t+1,k}(\omega)}, \ \ell \in \mathcal{L}, t \in \bar{\mathcal{T}}^-, k \in \bar{\mathcal{X}}^-, \omega \in \Omega \tag{3.11c}$$

$$f_{\ell,t,N_x}(\omega) = f_{\ell,t}^{out}(\omega), \ \ell \in \mathcal{L}, t \in \bar{\mathcal{T}}, \omega \in \Omega \tag{3.11d}$$

$$f_{\ell,t,1}(\omega) = f_{\ell,t}^{in}(\omega), \ \ell \in \mathcal{L}, t \in \bar{\mathcal{T}}, \omega \in \Omega \tag{3.11e}$$

$$p_{\ell,t,N_x}(\omega) = \theta_{rec(\ell),t}(\omega), \ \ell \in \mathcal{L}, t \in \bar{\mathcal{T}}, \omega \in \Omega \tag{3.11f}$$

$$p_{\ell,t,1}(\omega) = \theta_{snd(\ell),t}(\omega), \ \ell \in \mathcal{L}_p, t \in \bar{\mathcal{T}}, \omega \in \Omega \tag{3.11g}$$

$$p_{\ell,t,1}(\omega) = \theta_{snd(\ell),t}(\omega) + \Delta\theta_{\ell,t}(\omega), \ \ell \in \mathcal{L}_a, t \in \bar{\mathcal{T}}, \omega \in \Omega \tag{3.11h}$$

$$P_{\ell,t}(\omega) = c_4 \, f_{\ell,t}^{in}(\omega) \left(\left(\frac{\theta_{snd(\ell),t}(\omega) + \Delta\theta_{\ell,t}(\omega)}{\theta_{snd(\ell),t}(\omega)} \right)^\beta - 1 \right), \ \ell \in \mathcal{L}_a, t \in \bar{\mathcal{T}}, \omega \in \Omega. \tag{3.11i}$$

The physical model is a DAE system. The dynamic states are the spatially discretized link pressures and flows with the corresponding spatially discretized PDEs (3.11b)-(3.11c) being the differential equations. The network equations (3.11a), boundary conditions (3.11d)-(3.11h), and compressor equations (3.11i) are algebraic equations. It also makes practical sense to assume that the boost pressures are controls and that the compressor power outputs are algebraic states because they are uniquely defined the the compressor equations (3.11i). Note, however, that supply and demand flows as well as node pressures can act as either algebraic states or controls. In addition, it is not clear that the dummy flows are uniquely defined by the boundary conditions and network equations. These complications are important because it is necessary to specify consistent initial conditions for the DAE system. In addition, properly defining the controls will become important in Section 4.3 to correctly define the so-called nonanticipativity constraints for the controls. These constraints force the system to reach the same state for all scenarios at a given point in time.

To check for the consistency of the model and identify suitable initial conditions, we first perform a DOF analysis for a steady-state model. This can be obtained by taking the first time step of (3.11) and set derivatives with respect to time to zero. We also consider a single scenario and ignore the compressor equations (3.11i). This can be done without loss of generality because, for each compressor equation, there exists an additional power variable $P_{\ell,t}(\omega)$. We have $2|\mathcal{L}|+|\mathcal{S}|+|\mathcal{D}|$ variables given by $f_{\ell,1}^{in}$, $f_{\ell,1}^{out}$, $s_{i,1}$, and $d_{j,1}$, respectively. The discretized link flows $f_{\ell,1,k}$ and pressures $p_{\ell,1,k}$ give rise to an additional $2|\mathcal{L}|N_x$ variables. We also have $|\mathcal{N}|$ variables corresponding to the node pressures $\theta_{n,1}$ and $|\mathcal{L}_a|$ variables corresponding to the boost pressures $\Delta\theta_{\ell,1}$ for the active links. This gives a total of $2|\mathcal{L}|N_x + 2|\mathcal{L}| + |\mathcal{N}| + |\mathcal{S}| + |\mathcal{D}| + |\mathcal{L}_a|$ variables. The network balance comprises $|\mathcal{N}|$ equations, the discretized PDEs yield $2|\mathcal{L}|(N_x-1)$ equations, and the boundary conditions comprise $4|\mathcal{L}|$ equations. We thus have a total of $2|\mathcal{L}|N_x+2|\mathcal{L}|+|\mathcal{N}|$ equations and $|\mathcal{S}| + |\mathcal{D}| + |\mathcal{L}_a|$ DOF. In a practical setting, pressures at the supply nodes and demand flows are fixed. Imposing these two conditions reduces the number of DOF to $|\mathcal{L}_a|$, which are the boost pressures which

we can use as controls.

The steady-state analysis implies that we can achieve model consistency (i.e., fully specify the model with zero DOF) by fixing supply pressures, demand flows, and boost pressures. Note also that fixing these variables automatically renders supply flows and demand pressures as algebraic states. We also note that, if boost pressures are free and demand pressures are fixed in addition to demand flows then the number of DOF is reduced to $|\mathcal{L}_a| - |\mathcal{D}|$ and this can significantly constrain the operational flexibility. This is important as it indicates that fixing demand flows and pressures would be impossible unless the system has a large number of compressors. In Section 4 we discuss strategies to increase model flexibility by using softening constraints.

Based on the steady-state analysis, we can also conclude that all that is needed to fully define a steady-state of the system is to fix supply pressures, demand flows, and boost pressures and we need to impose the steady-state equations. This requires a total of $2|\mathcal{L}|N_x + 2|\mathcal{L}| + |\mathcal{N}| + |\mathcal{S}| + |\mathcal{D}| + |\mathcal{L}_a|$ equations. We now analyse the discretized dynamic model (3.11) over the entire time horizon. From the steady-state analysis we see that, if supply pressures and demand flows are fixed throughout the time horizon, we require $|\mathcal{L}_a|(N_t - 1)$ DOF for the dynamic model to be consistent. This is because the initial conditions for the boost pressures are given. From (3.11) we see that we have a total of $|\mathcal{N}|N_t + 2|\mathcal{L}|N_t + |\mathcal{S}|N_t + |\mathcal{D}|N_t + |\mathcal{L}_a|N_t + 2|\mathcal{L}|N_x N_t$ variables and $|\mathcal{N}|N_t + 2|\mathcal{L}|(N_x - 1)(N_t - 1) + 4|\mathcal{L}|N_t + 2|\mathcal{L}|N_x$ equations. The last quantity equals $|\mathcal{N}|N_t + 2|\mathcal{L}|N_x N_t + 2|\mathcal{L}|N_t - 2|\mathcal{L}|(N_x - 1)$ equations. If we specify $2|\mathcal{L}|(N_x - 1)$ initial conditions, then we have $|\mathcal{N}|N_t + 2|\mathcal{L}|N_x N_t + 2|\mathcal{L}|N_t$ equations, and these give $(|\mathcal{S}| + |\mathcal{D}| + |\mathcal{L}_a|)N_t$ DOF. By fixing supply pressures and demand flows for the entire time horizon and by fixing the boost pressures for the first time step, we obtain $|\mathcal{L}_a|(N_t - 1)$ DOF, as desired. We thus conclude that it is necessary to specify $2|\mathcal{L}|(N_x - 1)$ initial conditions for the full dynamic model (3.11) to be consistent. Note that we do not fix the initial conditions for the entire discretized profiles $f_{\ell,1,k}(\omega)$, $p_{\ell,1,k}(\omega)$ because doing so would entail $2|\mathcal{L}|N_x$ equations -$2|\mathcal{L}|$ more than necessary. The reason is that the boundary conditions introduce connectivity between the profiles. In Section 4.2 we discuss a couple of strategies to consistently specify the initial conditions.

We remark that in a practical setting, boost pressures (or compressor power) are in closed-loop with the discharge pressures of the compressors and the discharge pressure set-points are used controls. This setting is suggested in [3]. In the setting proposed here, we use the boost pressures as controls in order to avoid the need to model feedback loops.

4 Stochastic Optimal Control Model

In this section we describe the objective function, physical constraints, and initial conditions of the optimal control model.

4.1 Objective Function

We assume that the cost function for scenario ω has the following form

$$
\begin{aligned}
\varphi(\omega) = &\sum_{t\in\bar{\mathcal{T}}}\sum_{\ell\in\mathcal{L}_a} c_{e,t}P_{\ell,t}(\omega)\Delta\tau + \sum_{t\in\bar{\mathcal{T}}}\sum_{i\in\mathcal{D}} c_d(d_{j,t}(\omega) - \bar{d}_{j,t}(\omega))^2\Delta\tau \\
&+ \sum_{k\in\bar{\mathcal{X}}}\sum_{\ell\in\mathcal{L}} c_T(p_{\ell,T,k}(\omega) - p_{\ell,1,k}(\omega))^2\Delta x_\ell + \sum_{k\in\bar{\mathcal{X}}}\sum_{\ell\in\mathcal{L}} c_T(f_{\ell,T,k}(\omega) - f_{\ell,1,k}(\omega))^2\Delta x_\ell, \quad \omega\in\Omega. \quad (4.12)
\end{aligned}
$$

The first term is the total compressor cost over the horizon where $c_{e,t}$ is the compression cost at time step t. The second term penalizes deviations of the demands $d_{j,t}(\omega)$ from the desired signals $\bar{d}_{j,t}(\omega)$ and c_d as the penalty factor. Here, we assume that the demand signals are random. The model can be generalized to include compressor failures and other uncertain externalities but we focus on the demand case in order to simplify the presentation. The last two terms penalize deviations of the final flow and pressure axial profiles $p_{\ell,T,k}(\omega), f_{\ell,T,k}(\omega)$ from the initial axial profiles $p_{\ell,1,k}(\omega), f_{\ell,1,k}(\omega)$ and c_T is the penalty cost. These terminal constraints are typically required by operators to return the system to the original state. In the absence of these terminal constraints, the system will tend to deplete the line-pack inventory stored in the pipelines to minimize compression, leaving the system in a risky position for the next planning horizon [9]. This raises the issue of what is an appropriate initial steady-state for the system. We discuss this issue further in Section 4.2 as it pertains to the specification of the initial conditions. We emphasize that the terminal constraints are enforced by a penalty approach as opposed to the use of equality constraints. The latter approach would entail imposing $2|\mathcal{L}|N_x$ equations, but the model has only $|\mathcal{L}_a|(N_t - 1)$ degrees of freedom; consequently, we would need a time horizon with as many steps as the number of spatial points for the links in order to have any DOF left, clearly an impractical solution. In Section 5 we demonstrate that the penalty term is sufficient in practice to return the system to the initial state even for short time horizons.

In a stochastic optimization setting, one typically minimizes the expected value of the cost $\varphi(\omega)$. This approach assumes that the decision-maker (operator) is risk-neutral. It is also possible, however, to incorporate risk metrics to account for risk-averse decision makers. This approach can help the decision maker obtain operating policies that mitigate cost variance (volatility). Here, we use the conditional-value-at-risk (CVaR) metric because it is amenable to optimization [21]. We define a weighted sum of the expected value and CVaR metric (risk-mean) as the objective function. This is given by,

$$\Psi = (1 - \xi)\mathbb{E}\left[\varphi(\omega)\right] + \xi\text{CVaR}\left[\varphi(\omega)\right]. \tag{4.13}$$

Here,

$$\text{CVaR}\left[\varphi(\omega)\right] = \min_{\nu}\left[\nu + \frac{1}{1 - \sigma}\mathbb{E}\left[\varphi(\omega) - \nu\right]_+\right], \tag{4.14}$$

$\xi \in [0, 1]$ is the weighting factor, and σ is the confidence level.

4.2 Constraints

In a typical operational setting, the supply pressures are fixed (because the operator has no control over them), and demand flows are required to be satisfied strictly. We impose only the following on the supply pressures,

$$\theta_{sup(i),t}(\omega) = \bar{\theta}_i^{sup}, \ i \in \mathcal{S}, t \in \bar{\mathcal{T}}, \omega \in \Omega, \tag{4.15}$$

and we implicitly fix the demand signals through the penalty term in (4.12). By allowing demands to be free, the number of DOF increases to $\mathcal{L}_a(N_t - 1) + |\mathcal{D}|N_t$ per scenario. Although the demands are penalized, this flexibility is important because strictly enforcing demands during dynamic transitions is difficult. The quadratic term is also beneficial because it adds positive curvature to the Hessian matrix and it allows us to identify infeasible scenarios.

From the DOF analysis we have determined that, for the model to be consistent, we need to fix supply pressures and demand flows for the entire horizon, set the boost pressures for the first time step, and

7

specify $2|\mathcal{L}|(N_x - 1)$ initial conditions. If we do this naively, we would be tempted to specify the entire axial profiles for flows and pressures at the initial time step. This would lead, however, to $2|\mathcal{L}|N_x$ equations, and we would need to drop $2|\mathcal{L}|$ equations. Dropping boundary conditions is nontrivial because they set the connection between the dummy flows and link flows and the connection between node pressures and link pressures. We can achieve consistent initial conditions by simply dropping the first or last element of the initial pressure and flow profiles. In this case we will drop the last element. We thus append following set of equations to the full dynamic model (3.11),

$$\Delta\theta_{\ell,1}(\omega) = \Delta\theta_\ell^0, \ \ell \in \mathcal{L}_a, \omega \in \Omega \tag{4.16a}$$

$$f_{\ell,1,k}(\omega) = f_{\ell,k}^0, \ \ell \in \mathcal{L}, k \in \bar{\mathcal{X}}^-, \omega \in \Omega \tag{4.16b}$$

$$p_{\ell,1,k}(\omega) = p_{\ell,k}^0, \ \ell \in \mathcal{L}, k \in \bar{\mathcal{X}}^-, \omega \in \Omega \tag{4.16c}$$

in addition to (4.15) to fix the supply pressures and the penalty term to fix the demand flows. Here, $\Delta\theta_\ell^0, f_{\ell,k}^0, p_{\ell,k}^0$ are the initial conditions. For the initial conditions to be consistent, these must satisfy the algebraic equations (network and boundary conditions) of the dynamic model (3.11). We can find consistent initial conditions by solving the steady-state version of (3.11) with fixed boost pressures, supply pressures, and demands flows.

A much more convenient and direct way of finding consistent initial conditions is to directly append the following steady-state equations to the dynamic model (3.11),

$$\Delta\theta_{\ell,1}(\omega) = \Delta\theta_\ell^0, \ \ell \in \mathcal{L}_a, \omega \in \Omega \tag{4.17a}$$

$$0 = -c_{1,\ell}\frac{f_{\ell,1,k+1}(\omega) - f_{\ell,1,k}(\omega)}{\Delta x_\ell}, \ \ell \in \mathcal{L}, x \in \bar{\mathcal{X}}^-, \omega \in \Omega \tag{4.17b}$$

$$0 = -c_{2,\ell}\frac{p_{\ell,1,k+1}(\omega) - p_{\ell,1,k}(\omega)}{\Delta x_\ell} - c_{3,\ell}\frac{f_{\ell,1,k}(\omega)|f_{\ell,1,k}(\omega)|}{p_{\ell,1,k}(\omega)}, \ \ell \in \mathcal{L}, x \in \bar{\mathcal{X}}^-, \omega \in \Omega. \tag{4.17c}$$

Equations (4.17) fully specify the initial steady-state because the supply pressures are fixed from (4.15) and the demand flows are implicitly fixed through the penalty term. This formulation has an additional advantage: it might be of interest to the operator to simultaneously determine an optimal initial steady-state (and thus terminal steady-state) to aid the dynamic policies in the horizon (e.g., to strategically allocate initial inventory in the network). This can be done by dropping the initial conditions of the boost pressures (4.17a).

We also impose the following bounds for the compressors and demand pressures:

$$P_\ell^L \leq P_{\ell,t}(\omega) \leq P_\ell^U, \ \ell \in \mathcal{L}_a, t \in \bar{\mathcal{T}}, \omega \in \Omega \tag{4.18a}$$

$$\theta_\ell^{suc,L} \leq \theta_{snd(\ell),t}(\omega) \leq \theta_\ell^{suc,U}, \ \ell \in \mathcal{L}_a, t \in \bar{\mathcal{T}}, \omega \in \Omega \tag{4.18b}$$

$$\theta_\ell^{dis,L} \leq \theta_{snd(\ell),t}(\omega) + \Delta\theta_{snd(\ell),t}(\omega) \leq \theta_\ell^{dis,U}, \ \ell \in \mathcal{L}_a, t \in \bar{\mathcal{T}}, \omega \in \Omega \tag{4.18c}$$

$$\theta_j^L \leq \theta_{dem(j),t}(\omega) \leq \theta_j^{dem,U}, \ j \in \mathcal{D}, t \in \bar{\mathcal{T}}, \omega \in \Omega. \tag{4.18d}$$

The first set of bounds gives the minimum and maximum compressor power at each active link. A nonzero lower bound indicates that a compressor must run because of equipment protection reasons. The second set of bounds imposes minimum and maximum suction pressures for the compressors. The third set of bounds impose minimum and maximum discharge pressures for the compressors. The fourth set of bounds imposes minimum and maximum pressure at the demand nodes. Note that this range can be narrow.

4.3 Formulations

The discretized optimal control model is an NLP with the following structure

$$
\begin{array}{ll}
\min & \text{Risk-Mean Objective (4.13)} \\
\text{s.t.} & \text{Physical Model (3.11)} \\
& \text{Supply Pressures (4.15)} \\
& \text{Initial Conditions (4.16) or (4.17)} \\
& \text{Bounds (4.18).}
\end{array}
$$

From the DOF analysis we have that the control variables in this problem are the boost pressures $\Delta\theta_{\ell,t}(\omega)$ and the demand profiles $d_{j,t}(\omega)$ but the latter are fixed implicitly through the penalty term in the objective function. Putting all the scenarios together gives a total of $|\Omega||\mathcal{L}_a|(N_t - 1)$ DOF. Solving this problem (with weight $\xi = 0$ in the objective (4.13)) yields a *wait-and-see* (WS) solution. The WS setting is an ideal setting in which it is assumed that we can obtain a different control policy for each scenario (i.e., we have perfect information at the moment of decision) [2]. In a real setting, however, the operator needs to obtain a single control policy (make a decision now) in preparation for the uncertain future demands. We denote $T^d \leq N_t$ as the decision time step at which uncertainty is revealed. Before this time, system operation must remain the same for all scenarios up to time step T^d. In other words, the dynamic system must reach the same state for all scenarios at time T^d for the model to be consistent. From the DOF analysis we know that we can achieve this by enforcing the boost pressures to be equal accross scenarios. We thus add the following nonanticipativity constraints,

$$
\Delta\theta_{\ell,t}(\omega) = \mathbb{E}\left[\Delta\theta_{\ell,t}(\omega)\right], \ \ell \in \mathcal{L}_a, t \in \{1..T^d\}, \omega \in \Omega \setminus \{1\} \tag{4.19}
$$

Note that beyond time step T^d, the boost pressures are allowed to be scenario independent. In addition, adding the nonanticipativity constraints reduces the number of degrees of freedom to $|\mathcal{L}_a|(T_d - 1) + |\Omega||\mathcal{L}_a|(N_t - T_d)$. If $T_d = N_t$ we obtain a single control policy over the entire horizon and the problem will become infeasible because the demands will not be able to be fulfilled for each scenario.

Imposing the nonanticipativity constraints on the model (with $\xi = 0$) yields the so-called *here-and-now* (HN) solution. In the following, we will refer to the CVaR solution as the solution of the optimization model that enforces the nonanticipativity constraints and uses a non-zero weight ξ.

We remark that the optimization model follows a two-stage setting in which the first-stage involves time steps up to the decision time step T^d and the second stage involves the recourse actions taken after the decision time when uncertainty unfolds until the end of the horizon N_t. This implicitly assumes that uncertain demand profiles for $t = T_d + 1, ..., N_t$ reveal simulatenously for the second time period and not progressively at each time step, which would yield a multi-stage formulations. Consequently, the two-stage structure is more restrictive but also computationally more tractable.

We also define the *deterministic* solution of the optimization model. Here, the control policy up to time T^d is computed by assuming that the expected value of the demands is realized in the second-stage. We then fix the first-stage policy to evaluate the second-stage policies using the actual scenarios. We also consider the *worst-case* (WC) solution in which we compute the policy up to T^d by assuming that the worst scenario (in terms of cost) is realized in the second-stage. We then fix this policy to evaluate the second-stage policies using the actual scenarios.
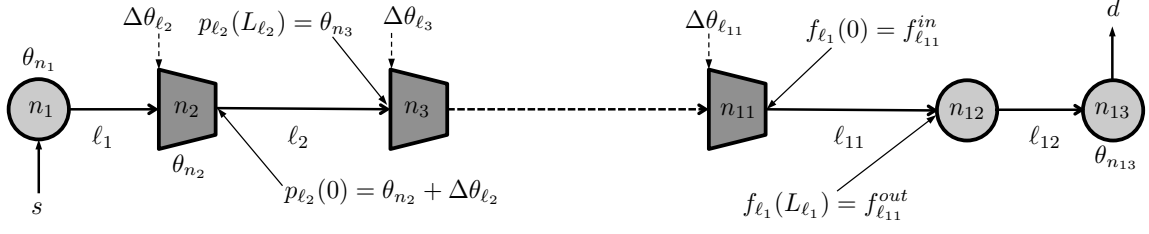
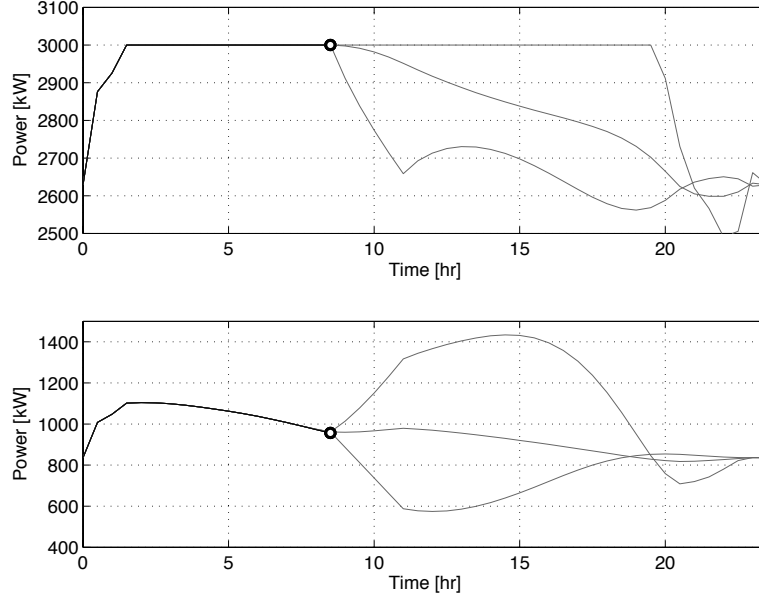Figure 1: Schematic representation of gas network system.

Figure 2: Optimal compressor power profiles for first (top) and second (bottom) compressors. Here-and-now solution.

5   Computational Study

We consider the network system sketched in Figure 1. The system comprises $|\mathcal{N}| = 13$ nodes, $|\mathcal{L}| = 12$ links ($|\mathcal{L}_a| = 10$ compressors), $|\mathcal{S}| = 1$ supply flow located at the first node, and $|\mathcal{D}| = 1$ demand flow located at the last node. The system spans 1,600 km with 36 inch (914 mm) pipes. The distance between compressors is 100 km. The pressure at the demand node (θ_{n_1}) should be maintained at least at 39 bar (565 psia) with a nominal demand flow of 24×10^6 SCM/day. The pressure at the supply point is 57 bar (827 psia). The minimum suction pressure for the compressors is 34 bar (493 psia). The maximum power available for the compressors is 3,000 kW, and we set the cost of compression to 0.10 \$/kWh.

We consider a planning horizon T of 24 hours discretized in $N_t = 48$ time intervals $\Delta\tau$ of 30 min (1800 sec). The decision time step T_d is set to 20 (9.5 hours into the horizon). Each link is discretized in space by using $N_x = 10$ points. We consider three demand profile scenarios. The demand from the initial time up to decision time remains at the nominal value of 10×10^6 SCM/day. At the decision time T^d it can increase to either $\{11, 12, 13\} \times 10^6$ SCM/day for 5 hours (10 time steps), then it returns to the original value at time T^{end}. Essentially, these events are step functions. We will refer to these scenarios as the low, medium, and

10

high demand scenarios, respectively. Note that the high demand scenario raises the demand by 30% above the nominal value. These types of events are typical of systems delivering gas to peaking power plants that can quickly come on-line with little or no notice [3].

The resulting NLPs are implemented in the algebraic modeling language AMPL [10] to obtain exact first and second order derivatives. The NLPs are solved by using the interior-point solver IPOPT with an adaptive barrier strategy [25, 17]. All problems are solved to a tolerance of 1×10^{-8}. MA57 is used as the sparse linear solver and we use the nested dissection strategy implemented in METIS to perform reordering [8, 12, 26, 27]. The AMPL model and data for this case study can be obtained from `http://www.mcs.anl.gov/~vzavala/PDEGasModel.tgz`. All computations were performed on a 2.7GHz processor with 16MB of memory and running Linux.

5.1 Model Behavior and Performance

We first discuss the behavior of the model in order to demonstrate its features and consistency. We start by considering the optimal time profiles for the first two compressors of the HN solution. These are presented in Figure 2. Note that prior to T^d, the compressor policy is the same in all scenarios. At the decision time, the profiles become scenario-dependent, and they eventually return to the same initial point. This demonstrates that imposing terminal constraints on the axial profiles is sufficient to define the final point for all states (both algebraic and dynamic) and controls.
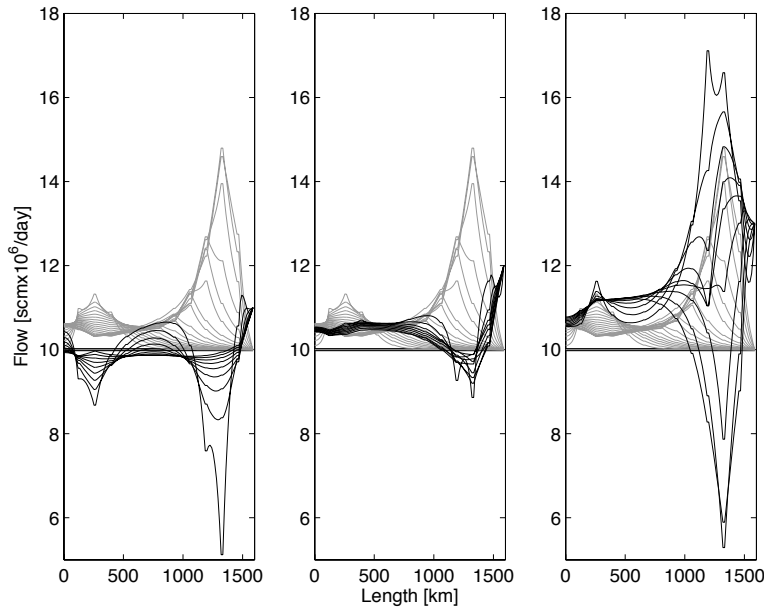

Figure 3: Optimal axial flow profiles for low (left), medium (middle), and high (right) demand scenarios. Here-and-now solution.
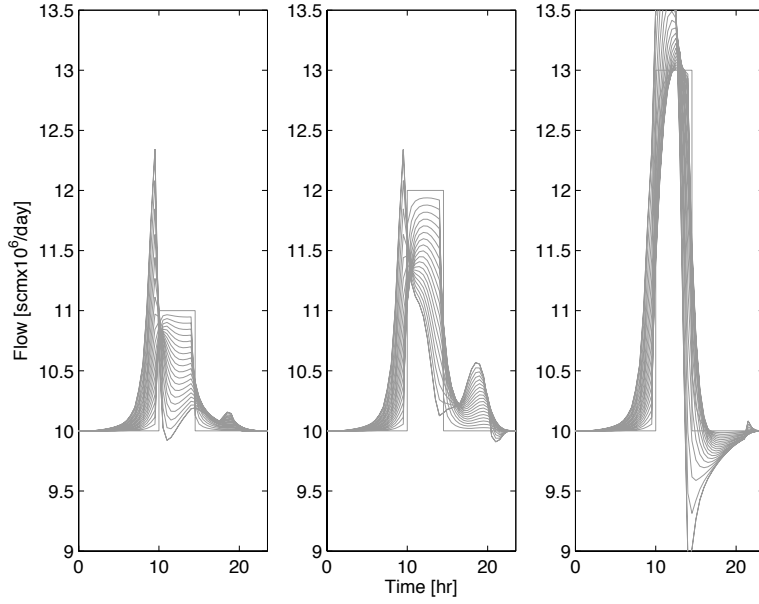
Figure 4: Optimal time profiles for flow in last link for low (left), medium (middle), and high (right) demand scenarios. Here-and-now solution.

In Figure 3 we present the axial flow profiles for the entire network for the three scenarios. The gray lines are the profiles prior to time T^d, and the black lines are the profiles during the period of increased demands (from T^d to T^{end}). The axial profiles prior to T^d are the same for the scenarios demonstrating that the nonanticipativity constraints and initial conditions are consistent. In addition, demand is satisfied at each time step for all scenarios. This can also be seen in Figure 4 in which we present time profiles for the flows at each spatial point in the last link. Note that the flow profile at the boundary of the system (black line) is capable of tracking the step changes in the demands exactly in all scenarios.

From Figure 3 we can see that the optimal HN policy consists on progressively accumulate line-pack toward the end of the system reflected by a large increase of flow close to the demand node. Once uncertainty is revealed, the system takes three different paths. To understand the optimal policies in more detail, in Figures 5 and 6 we present the axial flow and pressure profiles at T^d (right before demand increases), at the subsequent time step $T^d + 1$ (when uncertainty is revealed), and at the end of the increased demand period T^{end} (when demand returns to original level). From the high demand scenario we note that even if inventory is built up, flow needs to be increased further at the next time step to satisfy the demand at $T^d + 1$. This is accomplished by increasing the compression rates in the last two stations. At T^{end}, however, the inventory is released in order to minimize compression and start moving the system to the original low demand level. This is accomplished by flattening the pressure profile (shut down compression) close to the end of the system. Note that the drop in compression power at the last two stations triggers a complex flow profile upstream, illustrating the complex physical behavior of the system. For the low demand scenario, the inventory built prior to T^d is sufficient to satisfy demand and this is accomplished by progressively flattening the pressure profiles to release the inventory. The medium demand scenario exhibits a similar profile except that the pressure profile is not flattened as quickly and thus requiring more compression power to have a controlled release of inventory. The total compression energy for the low, medium, and high demand scenarios is 92742 kWh, 99783 kWh, and 113672 kWh, respectively.
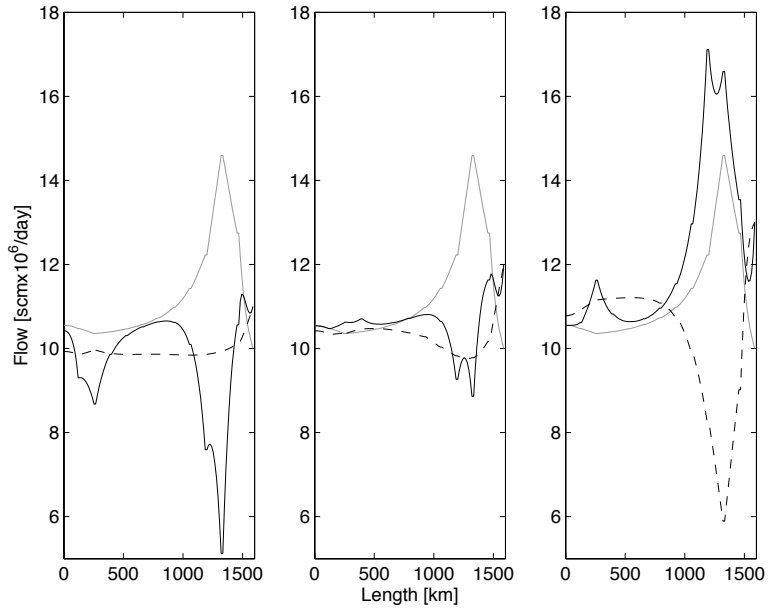
12

Figure 5: Optimal flow profiles for low (left), medium (middle), and high (right) demand scenarios. Gray line is profile at decision time T^d, black line is profile at $T^d + 1$ (30 minutes later), dashed line is profile at T^{end}.
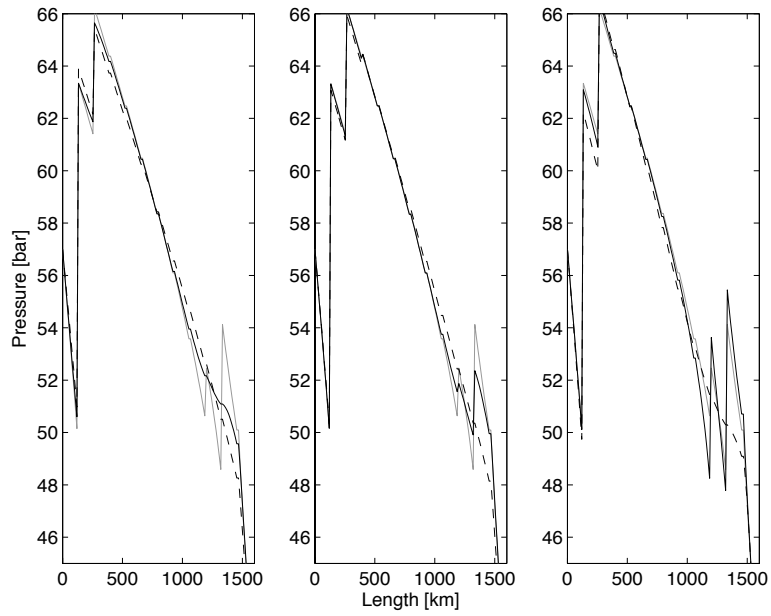

Figure 6: Optimal pressure profiles for low (left), medium (middle), and high (right) demand scenarios. Gray line is profile at decision time T^d, black line is profile at t$T^d + 1$ (30 minutes later), dashed line is profile at T^{end}.
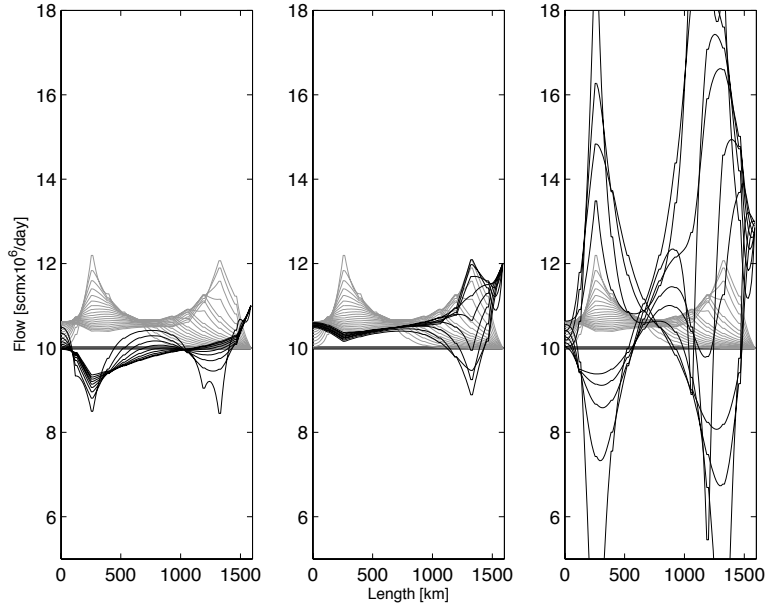
Figure 7: Optimal axial flow profiles for low (left), medium (middle), and high (right) demand scenarios. Deterministic solution.
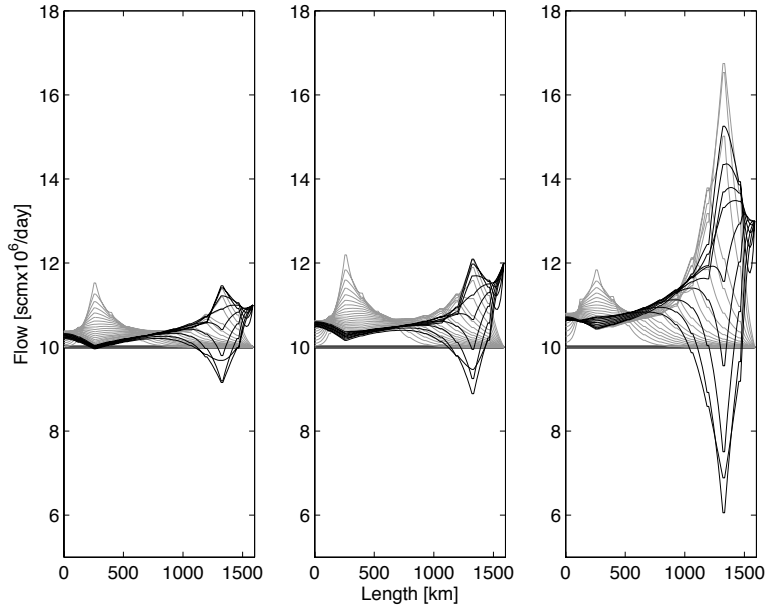

Figure 8: Optimal axial flow profiles for low (left), medium (middle), and high (right) demand scenarios. Wait-and-see solution.

5.2 Comparison of Formulations

We now compare the performance of the WS, HN, WC, CVaR, and deterministic formulations. The optimal flow profiles for the deterministic formulation are presented in Figure 7. The policy does not build as much inventory as does the HN solution presented in Figure 3. As a result, while the low and medium demand scenarios are feasible, the system struggles to satisfy the high demand scenario. In fact, we have found

14

that the demand needs to be curtailed for the system to remain feasible. This high-stress behavior is also reflected in highly volatile flow profiles resulting from aggresive recourse actions.

The axial flow profiles for the WS solution are presented in Figure 8. As can be seen, the profiles are similar to those of the HN solution presented in Figure 3. The ideal WS solution, however, presents less volatile profiles than those of the HN counterpart because it does not need to start from a common profile at T^d toward the profiles for the different scenarios, as in the HN policy. In particular, the WS axial profiles prior to T^d are different for each scenario, giving the system more flexibility. In other words, inventory can be planned differently for each scenario because we have perfect information. This is particularly evident in the low and high demand scenarios. The total power consumed in the WS scenarios are 88245 kWh, 98914 kWh, and 112779 kWh, respectively. This is less than 1% per scenario, compared with the HN solution. Clearly, significant robustness can be gained by using the HN formulation over the deterministic one without sacrificing much performance over the ideal case of perfect information.

In practice, operators are risk-averse and can act conservatively to ensure that the system can fulfill high demand scenarios. To capture this behavior, we now compare the HN solution with the WC solution. In Figure 9, we present the axial profiles for the WC solution in which the system is prepared defensively for the period of high demand. In this case, the high demand scenario is feasible. Note, however, that the low demand scenario now exhibits a high degree of volatility because the system needs to move rapidly from a point of very high inventory to a point of low demand. The total power consumed in the WC scenarios is 96063 kWh, 100938 kWh, and 112779 kWh, respectively. Note that the WC solution leads to more expensive operations particularly for the low demand scenario. While the difference in performance compared with that of the HN policy is not exorbitant in this case study, the issue of solution volatility induced by the robust formulation can be undesirable to the operator. We should also highlight that, as seen in the results, the worst-case approach can place the system at a far-distant state from which it might not recover because of dynamic limitations.

Table 1: Comparison of formulations in terms of total energy consumed.

Formulation	Compression Energy (kWh)
WS	88245, 98914, 112779
HN	92742, 99783, 113672
WC	96063, 100938,112779
CVaR (ξ=0.25)	93075, 99910, 113351
CVaR (ξ=0.50)	93692, 100150, 113061
CVaR (ξ=0.75)	94572, 100496, 112856
CVaR (ξ=0.90)	95217, 100729, 112797

To allow for a more systematic management of risk, we now introduce the CVaR metric into the cost function. In Figure 10 we present the axial profiles for a weighting parameter $\xi = 0.5$ (equal weight between expected value and CVaR value). Compared with the HN solution of Figure 3, the CVaR metric can decrease the volatility of the profiles in the extreme (low and high demand) scenarios. The total power consumed in this case is 93692 kWh, 100150 kWh, and 113061 kWh, lower than those obtained with the WC solution for the low and medium demand scenarios. The difference between the low and high demand scenarios is 19369 kWh, while for the HN solution it is 20930 kWh indicating that cost variability can be mitigated. As we increase the weight ξ toward one, the CVaR solution becomes more defensive and mimics the worst-

case solution. In Table 1 we present the total power consumed for the different formulations. We conclude that the CVaR formulation can help operators systematically adjust their risk-averseness and evaluate the impact of a given policy on economic performance and system behavior. Note also that the use of stochastic formulations is informative to the operator as it allows her/him to evaluate system dynamic behavior under a range of possible scenarios and to position the system at a "safe" state.
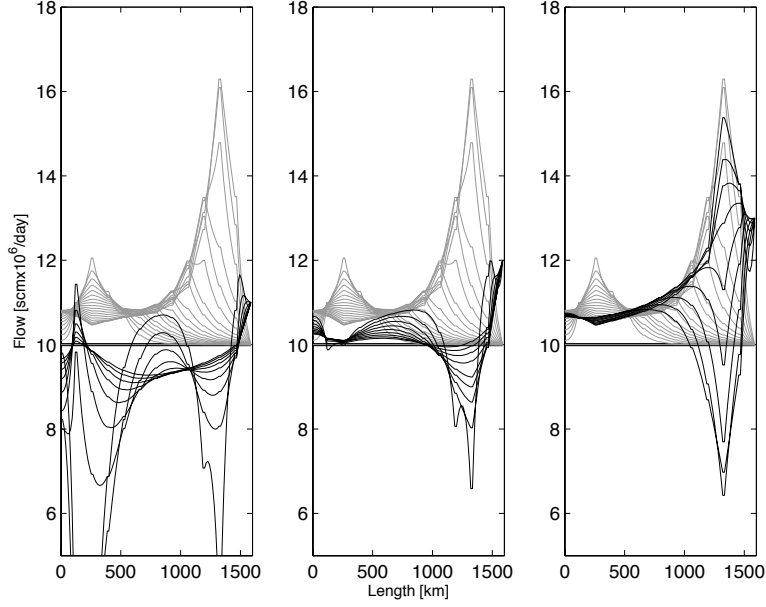

Figure 9: Optimal axial flow profiles for low (left), medium (middle), and high (right) demand scenarios. Worst-case solution.
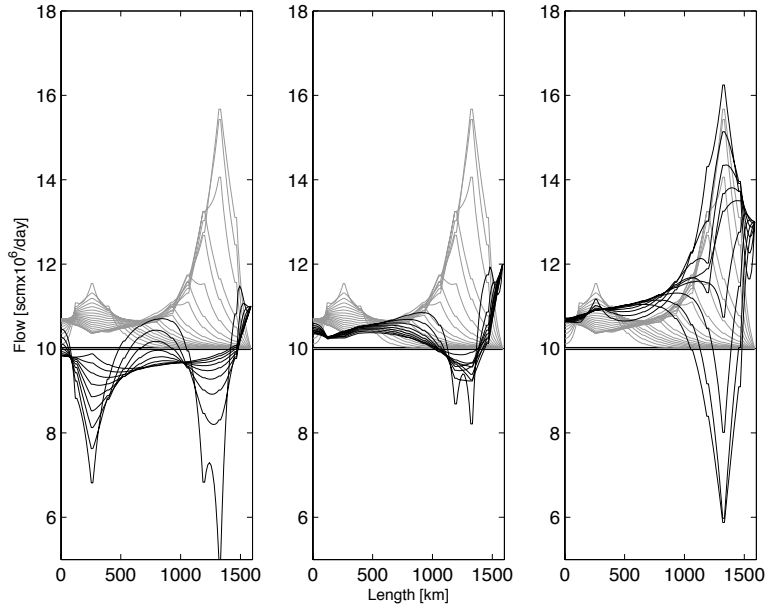

Figure 10: Optimal axial flow profiles for low (left), medium (middle), and high (right) demand scenarios. CVaR solution with $\xi = 0.5$.

5.3   Scalability Issues

Clearly, the optimal control model presented is computationally challenging. The first source of complexity is the presence of nonlinear PDEs in each link, which are in turn coupled through the network constraints. The second source of complexity is the number of scenarios, although well-established techniques are available for parallelization. Here, we report on the effects of the discretization mesh resolution and number of scenarios on the dimensions of the NLP, scalability, and economic performance.

Table 2: Effect of discretization resolution on computational and economic performance.

$\vert\Omega\vert$	N_x	n	m	Iterations	Time [min:sec]	Energy [kWh]
1	2	6278	5736	47	00:02	89566
1	6	13190	12600	45	00:10	98182
1	10	20102	19464	44	00:19	98914
1	20	37382	36624	45	00:45	99351
1	60	106502	105264	56	02:59	99612
1	100	175602	173904	58	05:43	99663
3	2	18832	17658	36	00:13	86391,91333,98294
3	10	60304	58832	52	03:18	92742,99783,113672
3	20	112144	110312	51	07:18	92464,99937,114327

Computational results are presented in Table 2. We first note that a problem with a high discretization resolution ($N_x = 100$) and a single scenario gives rise to an NLP with over 175,000 variables n and equality constraints m. NLPs of such dimensions (and over) are typical in optimal control of PDEs when a full discretization approach is used [22, 5, 26]. The solution time for the high-resolution problem is 6 minutes, and we can expect similar times for solving instances with more scenarios if linear algebra parallelization is implemented to split the scenarios. In particular, we note that the number of first-stage variables in this problem is less than 200 (given by the control policies of the 10 compressors up to time step $T^d = 20$). For problems with this number of first-stage variables, Schur decomposition exhibits nearly perfect speedups [14, 11, 28]. If we increase the number of compressors from 10 to 100 the number of first-stage variables will be on the order of 2,000 for which Schur decomposition can still achieve nearly perfect speedups. Note, however, that problems with over 200 compressors or longer first-stage periods (i.e., large T^d) will deteriorate scalability. We also note that even for a simple network with 13 nodes and 12 links and a single scenario, the solution times for a high-resolution problem are already on the order of 6 minutes. If we increase the number of links by a factor of 10 (from 12 to 120), we can expect NLPs with already 1,000,000 variables and solution times of over an hour (in the ideal case of linear scalability), which limits the model applicability in real-time environments. This points to the need to develop solution strategies that couple scenario decomposition with space-time decomposition schemes.

In the last three rows of Table 2 we present computational results for problems with 3 scenarios and 2 different discretization resolutions. The minimimum total energy computed for the case with 2 discretization points per link is underestimated by nearly 10-15% compared to the high resolution model of 20 discretization points. These coarse discretization schemes have been used in several studies [9, 16] and we should emphasize that they can have strong effects on economic performance. In addition, we have also observed that, because of the limited number of degrees fo freedom in the model, control policies obtained

with a low resolution discretization model are infeasible for high resolution models. This situation is manifested in the inability of the system to meet demand signals.

6 Conclusions and Future Directions

We have presented a stochastic optimal control model for natural gas network operations. The consistency of the model has been verified using a DOF analysis. We have found that the use of stochastic policies can significantly aid robustness in operations compared with deterministic policies. Robustness is particularly critical in gas networks because of the complex physical behavior propagating throughout the system and because of the limited degrees of freedom available for operation. We have also found that the use of risk metrics provide flexibility to the operator to mitigate system volatility. Our computational study suggests that off-the-shelf solvers are insufficient to solve problems of real complexity. This situation motivates interesting research directions. The complexity induced by the number of scenarios can be mitigated by using Schur decomposition strategies, as suggested in [14, 11, 28]. To deal with larger networks, however, one must couple Schur decomposition with advanced space-time discretization strategies [4] and strategies to perform time-space separation [23]. Modeling extensions are needed that account for more rigorous physics including nonisothermal operations in order to capture weather effects. Moreover, physical models must be developed for control elements such as valves. Additional developments are needed including multi-stage models and uncertainty characterizations of demand profiles by coupling with power grid dispatch operations.

Acknowledgments

A Nomenclature and Constants

The speed of sound in the gas (assuming an ideal gas behavior), the friction factor λ_ℓ, the gas isentropic expansion factor γ, and the compression coefficient β can be computed from,

$$\nu^2 = \frac{\gamma z R T_{gas}}{M} \qquad \lambda_\ell = \left(2 \log_{10}\left(\frac{3.7\, D_\ell}{\epsilon_\ell}\right)\right)^{-2} \qquad \gamma = \frac{c_p}{c_v} \qquad \beta = \frac{\gamma - 1}{\gamma},$$

where z is the gas compressibility factor, R is the universal gas constant, T_{gas} is the gas temperature, M is the gas molar mass, ϵ_ℓ is the pipe rugosity, and c_v is the heat capacity of the gas at constant volume. We also define the following auxiliary constants:

$$c_{1,\ell} = \frac{\nu^2}{A_\ell}\frac{\alpha_p}{\alpha_f} \qquad c_{2,\ell} = A_\ell \frac{\alpha_f}{\alpha_p} \qquad c_{3,\ell} = \frac{8\,\lambda_\ell\,\nu^2\,A_\ell}{\pi^2\,D_\ell^5}\frac{\alpha_p}{\alpha_f} \qquad c_4 = \frac{1}{\alpha_f}\,c_p\,T_{gas}.$$

Here, c_p is the gas heat capacity at constant pressure.

Table 3: Model variables and units.

Variable	Description	Units
τ	Time	s
x	Spatial dimension	m
ω	Scenario	-
ρ	Density inside pipe	$\frac{kg}{m^3}$
w	Speed inside pipe	$\frac{m}{s}$
q	Volumetric flow inside pipe	$\frac{m^3}{s}$
f	Flow inside pipe	$\frac{SCM \times 10^{-4}}{hr}$
p	Pressure inside pipe	bar
f^{in}	Pipe inlet flow	$\frac{SCM \times 10^{-4}}{hr}$
f^{out}	Pipe outlet flow	$\frac{SCM \times 10^{-4}}{hr}$
s	Supply flow	$\frac{SCM \times 10^{-4}}{hr}$
d	Demand flow	$\frac{SCM \times 10^{-4}}{hr}$
θ	Node pressures	bar
$\Delta\theta$	Compressor boost	bar
P	Compressor power	kW
φ	Cost function	$\$$
Ψ	Objective function	$\$$.

Table 4: Model parameters and units.

Parameter	Description	Units
T, T^d	Planning time, decision time	s
$\Delta\tau, \Delta x$	Time and space discretization interval length	s, m
ξ	Weighting parameter	-
ν	Speed of sound in gas	$\frac{m}{s}$
c_p, c_v	Gas heat capacities at constant pressure and volume	$2.34\frac{kJ}{kg\,K}, 1.85\frac{kJ}{kg\,K}$
γ, z	Gas isentropic expansion coefficient and compressibility	-
R	Universal gas constant	$8,314\frac{J}{kg_{mol}\,K}[=]\frac{Pa\,m^3}{kg_{mol},K}$
M	Gas molar mass	$18\frac{kg}{kg_{mol}}$
ρ_n	Gas density at normal conditions	$0.72\frac{kg}{m^3}$
T_{gas}	Gas temperature	$293.15\,K$
L, D, A	Pipe length, diameter, and transveral area	m, m, m^2
λ, ϵ	Friction coefficient and pipe rugosity	$-, m$
α_f	Scaling factor for flow	$\frac{3,600}{1\times10^4\rho_n}[=]\frac{SCM\times10^{-4}/hr}{kg/s}$
α_p	Scaling factor for pressure	$1\times10^{-5}\frac{bar}{Pa}$
c_t^e	Cost of compression	$\frac{0.1}{3600}\frac{\$}{kW-s}[=]\frac{\$}{kJ}$
c_1	Auxiliary constant	$\frac{bar/s}{SCM\times10^{-4}/hr-m}$
c_2	Auxiliary constant	$\frac{SCM\times10^{-4}/hr-s}{bar/s}$
c_3	Auxiliary constant	$\frac{bar}{SCM\times10^{-4}-s/hr}$
c_4	Auxiliary constant	$\frac{kW}{SCM\times10^{-4}/hr}$
c_d, c_T	Tracking cost for demands and terminal constrains	-
P^L, P^U	Lower and upper bounds for compressor power	kW
$\theta^{dem,L}, \theta^{dem,U}$	Lower and upper bounds for pressures at demand nodes	bar
$\theta^{suc,L}, \theta^{suc,U}$	Lower and upper bounds for suction pressures	bar
$\theta^{dis,L}, \theta^{dis,U}$	Lower and upper bounds for discharge pressures	bar
$\bar{\theta}^{sup}$	Supply pressure	bar
$\bar{d}$	Desired demand signal	$\frac{SCM\times10^{-4}}{hr}$
$\Delta\theta^0$	Initial conditions for boost pressures	bar
f^0	Initial conditions for scaled flows	$\frac{SCM\times10^{-4}}{hr}$
p^0	Initial conditions for scaled pressures	bar

References

[1] B. T. Baumrucker and L. T. Biegler. MPEC strategies for cost optimization of pipeline operations. *Computers & Chemical Engineering*, 34(6):900–913, 2010.

[2] J. R. Birge and F. V. Louveaux. *Introduction to stochastic programming*. Springer, 1997.

[3] R. G. Carter and H. H. Rachford Jr. Optimizing line-pack management to hedge against future load uncertainty. In *PSIG Annual Meeting*, 2003.

[4] D. Clever, J. Lang, S. Ulbrich, and C. Ziems. Generalized multilevel SQP-methods for pdae-constrained optimization based on space-time adaptive pdae solvers. In *Constrained Optimization and Optimal Control for Partial Differential Equations*, pages 51–74. Springer, 2012.

[5] F. E. Curtis, J. Huber, O. Schenk, and A. Wächter. A note on the implementation of an interior-point algorithm for nonlinear optimization with inexact step computations. *Mathematical programming*, 136(1):209–227, 2012.

[6] D. De Wolf and Y. Smeers. Optimal dimensioning of pipe networks with application to gas transmission networks. *Operations Research*, 44(4):596–608, 1996.

[7] D. De Wolf and Y. Smeers. The gas transmission problem solved by an extension of the simplex algorithm. *Management Science*, 46(11):1454–1465, 2000.

[8] I. S. Duff. Ma57—a code for the solution of sparse symmetric definite and indefinite systems. *ACM Transactions on Mathematical Software (TOMS)*, 30(2):118–144, 2004.

[9] K. Ehrhardt and M. C. Steinbach. *Nonlinear optimization in gas networks*. Springer, 2005.

[10] R. Fourer, D. M. Gay, and B. W. Kernighan. *AMPL*. Boyd and Fraser, 1993.

[11] J. Gondzio and A. Grothey. Exploiting structure in parallel implementation of interior point methods for optimization. *Computational Management Science*, 6(2):135–160, 2009.

[12] George Karypis and Vipin Kumar. Metis-unstructured graph partitioning and sparse matrix ordering system, version 2.0. 1995.

[13] C. Liu, M. Shahidehpour, Y. Fu, and Z. Li. Security-constrained unit commitment with natural gas transmission constraints. *IEEE Transactions on Power Systems*, 24(3):1523–1536, 2009.

[14] M. Lubin, C. G. Petra, M. Anitescu, and V. M. Zavala. Scalable stochastic optimization of complex energy systems. In *2011 International Conference for High Performance Computing, Networking, Storage and Analysis (SC)*, pages 1–10. IEEE, 2011.

[15] A. Martin, M. Möller, and S. Moritz. Mixed integer models for the stationary case of gas network optimization. *Mathematical Programming*, 105(2-3):563–582, 2006.

[16] S. Moritz. *A mixed integer approach for the transient case of gas network optimization*. PhD thesis, TU Darmstadt, 2007.

[17] J. Nocedal, A. Wächter, and R. A. Waltz. Adaptive barrier update strategies for nonlinear interior methods. *SIAM Journal on Optimization*, 19(4):1674–1693, 2009.

[18] R. P. O'Neill, M. Williard, B. Wilkins, and R. Pike. A mathematical programming model for allocation of natural gas. *Operations Research*, 27(5):857–873, 1979.

[19] A. Osiadacz. Simulation of transient gas flows in networks. *International Journal for Numerical Methods in Fluids*, 4(1):13–24, 1984.

[20] H. H. Rachford Jr and R. G. Carter. Optimizing pipeline control in transient gas flow. In *PSIG Annual Meeting*, 2000.

[21] R. T. Rockafellar and S. Uryasev. Optimization of conditional value-at-risk. *Journal of Risk*, 2:21–42, 2000.

[22] O. Schenk, A. Wächter, and M. Weiser. Inertia-revealing preconditioning for large-scale nonconvex constrained optimization. *SIAM Journal on Scientific Computing*, 31(2):939–960, 2008.

[23] M. C. Steinbach. On PDE solution in transient optimization of gas networks. *Journal of Computational and Applied Mathematics*, 203(2):345–361, 2007.

[24] J. K. Van Deen and S. R. Reintsema. Modelling of high-pressure gas transmission lines. *Applied Mathematical Modelling*, 7(4):268–273, 1983.

[25] A. Wächter and L. T. Biegler. On the implementation of an interior-point filter line-search algorithm for large-scale nonlinear programming. *Mathematical Programming*, 106(1):25–57, 2006.

[26] V. M. Zavala and L. T. Biegler. Nonlinear programming strategies for state estimation and model predictive control. In *Nonlinear model predictive control*, pages 419–432. Springer, 2009.

[27] V. M. Zavala and L. T. Biegler. Optimization-based strategies for the operation of low-density polyethylene tubular reactors: nonlinear model predictive control. *Computers & Chemical Engineering*, 33(10):1735–1746, 2009.

[28] V. M. Zavala, C. D. Laird, and L. T. Biegler. Interior-point decomposition approaches for parallel solution of large-scale nonlinear parameter estimation problems. *Chemical Engineering Science*, 63(19):4834–4845, 2008.